# Maximisation of sensitivity to Long Lived Particles with ANUBIS using a Monte Carlo based geometry optimisation

4634H

*Supervisor*
Dr. Oleg Brandt

May 16, 2022

**Abstract**

While the Standard Model (SM) is an extremely accurate theory describing most of physics, some fundamental questions are left unanswered, including those about Dark Matter (DM) existence and composition. This is where Beyond the SM (BSM) theories come in, trying to address unsolved issues, many of which predict the presence of particles with longer lifetimes than those typically observed at accelerators. As a consequence, understanding Long Lived Particles (LLPs) could prove crucial in the search for new physics, which is why many efforts at ATLAS and CMS are currently being directed towards detection of such LLPs. However, these efforts have had little success yet. The newly proposed ANUBIS (An Underground Belayed In-Shaft) detector, to be implemented at ATLAS, could prove crucial in extending the sensitivity to longer lifetimes thanks to Tracking Stations (TSs) placed at distances up to 80 m away from the Interaction Point (IP). In this work I employed Monte Carlo (MC) simulations to study the sensitivity of ANUBIS to Higgs decay-produced LLPs, in different geometric setups. In particular, I focused on an alternative configuration which involves instrumenting the ATLAS cavern ceiling with TSs, to cover as large a solid angle as possible while keeping the radial distance small. The results showed significant improvement in sensitivity when considering optimistic background estimates.

# Contents



# 1 Introduction

The Standard Model (SM) is an extremely successful theory that describes with great accuracy most aspects of fundamental physics. Yet, it leaves some unanswered puzzles such as the origin of neutrino masses, the matter-antimatter asymmetry and, in particular, the existence and properties of Dark Matter (DM), suggesting the presence of physics Beyond the Standard Model (BSM) [1].

Various theories with DM candidates have been proposed, trying to address the question on DM's nature, many of which predict the presence of new particles with longer lifetimes than those predicted by the SM. Such Long Lived Particles (LLP) are thus being searched for via different collider experiments which investigate their direct interaction with detectors or their decay products.
LLPs appear in various models of BSM physics, some notable examples being Supersymmetry (SUSY), Neutral Naturalness and Hidden Sector portals. In the following I will focus on the latter and, more specifically, on the Higgs Portal Model which features exotic decays of the Higgs boson into hidden sector LLPs [2]. In this scenario, the neutral LLPs of interest decay into SM particles, typically leaving a displaced vertex signature in the detector.

In Fig. 1 the current experimental constraints on Higgs decay to long lived scalars are shown as functions of the LLPs' decay length $c\tau$ [2]. Here, ATLAS [3], CMS [4] and LHCb [5] searches are considered. As it can be observed, for $c\tau \in [1, 10]$ m both

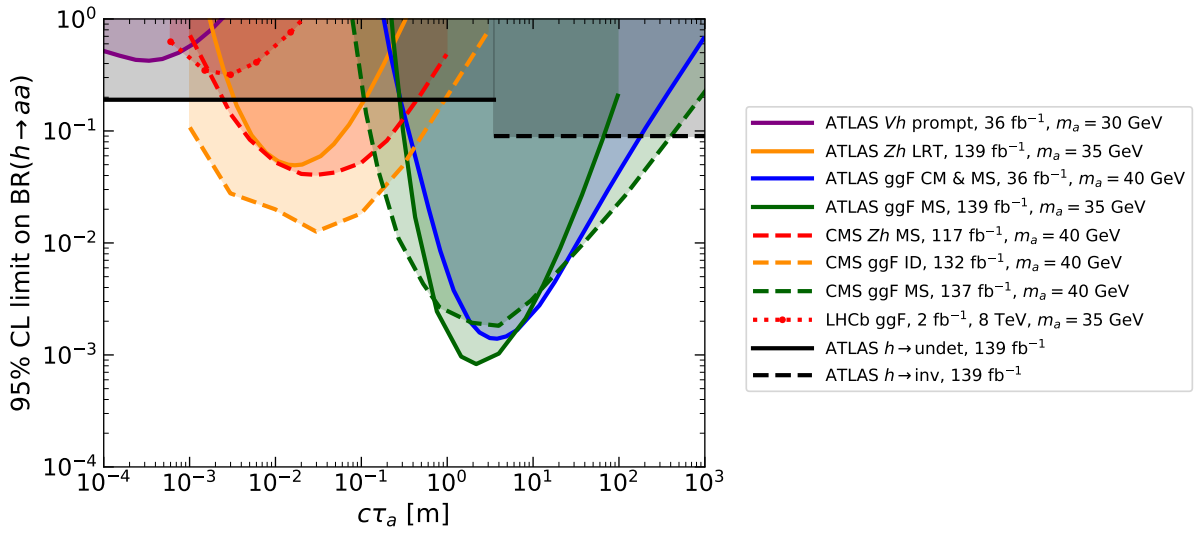


FIG. 1: 95% Confidence level on on exotic Higgs decay's branching ratio BR($h \to aa$) vs proper decay length $c\tau$ for ATLAS [3], CMS [4] and LHCb [5] searches [2].

CMS and ATLAS successfully constrain branching ratios (BRs) to $\lesssim 10^{-3}$. However, decay lengths $c\tau \gtrsim 10^3$ m have not been explored by any collider experiment, with the only current limit given by invisible Higgs decays. These will be explored by future detectors aiming at LLPs such as MATHUSLA [6], CODEX-b [7], FASER [8] and the object of this investigation: AN Underground Belayed In-Shaft (ANUBIS)[9]. In this work I focused on studying the sensitivity of ANUBIS to neutral LLPs produced in Higgs decay within different geometrical frames, with the ultimate purpose of finding the most optimised setup. Specifically, I implemented a set of new configurations of the detector and obtained their sensitivity estimates. My results are shown and analysed in Sec. 3

and Sec. 4.

# 2 Theoretical Background

## 2.1 Higgs BSM Models

To address the unsolved puzzles in our universe various BSM models have been formulated, many of which theorise the presence of new particles beyond the SM. Most ongoing searches for these new particles are currently focusing their efforts towards the study of prompt decays at colliders. However, particles with longer lifetimes are also great candidates for the unveiling of the mysteries of Particle Physics, as they are theorised to be characteristic of many BSM models.
Given this rising interest in LLPs, it is relevant to discuss how such particles can exist and how they can be practically employed in BSM research.

The lifetime $\tau$ of a particle of mass $M$ is given by the inverse of its decay rate

$$\frac{1}{\tau} = \Gamma \sim \frac{1}{M} \int |\mathcal{M}|^2 d\Pi \quad , \tag{1}$$

where $\mathcal{M}$ is the matrix element of the process and $d\Pi$ is the decay phase space. Therefore, a long lifetime can arise from either a very small phase space or suppressed matrix element. The former can originate from accidental degeneracies in the spectrum, as well as splitting of degenerate states by small breaking of an approximate symmetry. On the other hand, the matrix element for a decay process can be suppressed by a weak coupling between particles, or by an approximate symmetry which would, if precise, forbid the decay [10]. Such suppressions arise in multiple cases within the SM. One of these is Higgs boson decay which, even if not macroscopically long lived, has a much larger lifetime than the other massive bosons $W$ and $Z$. Its decay to fermions is in fact suppressed by small Yukawa couplings, while decays to pairs of gluons $gg$ and photons $\gamma\gamma$ by loop factors. The decay width is then dominated by $h \to b\bar{b}$ with a small Yukawa coupling $y_b = 0.02$ meaning that any other small couplings of the Higgs to light states will show additional decays modes with observable BRs [11].
Considering that BSM theories are usually characterised by such small couplings [6], and that LLPs are relevant in many BSM models, the discovery of the 125 GeV Higgs boson [12, 13] has paved the way to new BSM research, hinting at connections between the Higgs and the Dark Sector (DS) i.e. the hidden sector that contains the DM candidates. One of the theoretical motivations for such link is that the SM Higgs doublet is the only field that, assuming DM is not charged under the SM Gauge group, gives rise to a renormalisable coupling to the DS [2]. Many models involving Higgs connections to DM exist, such as

Higgs Portal, extended Higgs Portal, and models featuring exotic Higgs decays. In the two former models the Higgs boson directly serves, alone or combined with other spin-0 particles, as bridge (or portal) between the DS and the SM. The latter, on the other hand, are often characterised by the decay of the Higgs to neutral particles with longer lifetimes. Some of these models fall within the category of Neutral Naturalness, a set of frameworks which address the electroweak hierarchy problem [10] and includes twin Higgs [14], folded SUSY [15], and quirky little Higgs [16]. In this investigation I employed a simplified model of these, in which the SM Higgs decays to two neutral long lived scalars. These then decay to charged SM particles producing a displaced vertex signature which can be observed at detectors. Specifically, I considered SM Higgs produced via gluon-gluon fusion (GGF) and vector-boson fusion (VBF). The relevant Feynman Diagrams can be seen in Fig. 2.

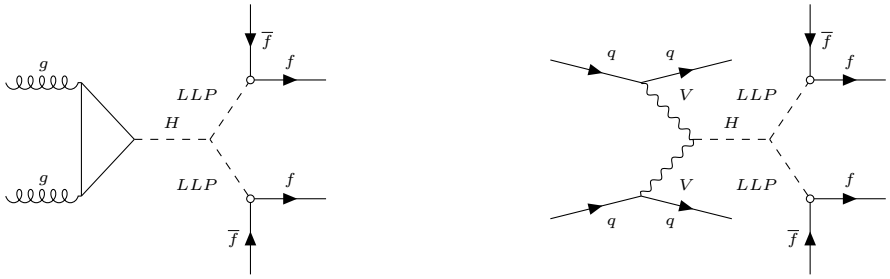


(a) (b)

FIG. 2: Feynman diagrams of Higgs production and decay via (a) GGF, (b) VBF.

## 2.2 LLPs at Collider Experiments

Current collider experiments and detectors are mainly built for SM particles' detection, but can be employed for LLP searches if their behaviour is known.

A typical collider experiment employs a series of multi-purpose detector subsystems, used to reconstruct as much information as possible about the produced particles. A schematic diagram is shown in Fig. 3 [17]. The first component of the detector is called inner detector (ID), which reconstructs charged particles' tracks via ionisation. The following sector is the calorimeter, which promotes electromagnetic and hadronic interactions to measure the particles' energy. The final subsystem is the muon spectrometer or muon system (MS). This accounts for muons' detection, and is there due to the fact that they experience little loss of energy when passing through the calorimeter and are thus not easily identifiable. Final states with very high energy or long enough lifetimes that manage to escape the detector are ultimately identified via missing transverse momentum $E_{\mathrm{T}}^{\mathrm{miss}}$. This is the difference between the initial and measured final momentum in the plane transverse to the beam direction which, if non-zero, implies the presence of invisible particles that carry

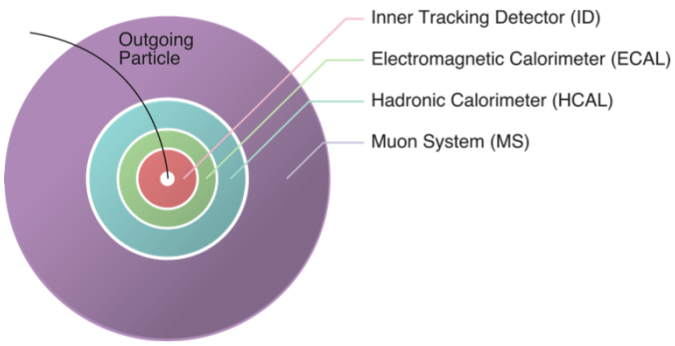


FIG. 3: Schematic diagram of a typical collision experiment detector [17].

momentum outside the active region.

Despite collider detectors being designed for SM particles, LLPs and their decay products do interact within them, leaving signatures specific to particles with long lifetimes. Due to their large decay lengths, the charged SM decay products of LLPs are characterised by having tracks in the detector that are displaced from the primary interaction vertex. The common origin of these tracks, known as the displaced vertex (DV), together with the displaced tracks themselves, are two of the most important LLP signatures in the detector. Delayed detector signals, due to slow-moving particles in the case of heavy LLPs, also play an important role in LLPs searches when the detector has high enough timing resolutions. Finally, missing momentum is also relevant for in some cases.

When looking for LLPs, one can perform measurements either along the beam line (on-axis), if interested in weakly coupled light particles, or orthogonal to it (off-axis), if looking at decays of heavy states. Many proposals of experiments have recently been developed aiming to exploit CERN facilities to look for LLPs in the latter of these two cases. One of these is MATHUSLA [6]. This collaboration suggests to instrument the surface 100 m away from the CMS (or ATLAS) interaction point (IP), with a large detector capable of reconstructing tracks and DV with high resolution. The main issues behind this ambitious project are its great size and requirement of controlled backgrounds as pointed out by [1]. CODEX-b [7] is another experiment that aims to observe light ($m \leq 10$ GeV) neutral LLPs via a shielded tracking detector placed 25 m away from LHCb. The need of a passive shield is what constitute a challenge for this proposal, as well as that of an upgrade of the LHCb high luminosity. On the other hand, FASER [8], sets out to search for light weakly coupled LLPs via a detector placed 480 m away from the ATLAS IP along the LHC beam line. While being a more complex proposal, involving scintillators, a spectrometer and electromagnetic calorimeter, both its size and costs are contained, making it a highly promising experiment.

### 2.2.1 ANUBIS

ANUBIS, the object of this investigation, is a newly proposed detector that aims to search for heavy mediated LLPs (off-axis) by exploiting and instrumenting the existing ATLAS PX14 service shaft to extend its searches to particles with lifetimes $c\tau > 10^3$ m [9]. The experiment plans to equip the shaft with four equally distanced circular Tracking Stations (TSs) (Fig. 4), consisting of 2 layers of detection Resistive Plate Chambers (RPC) technology sheets which employ gaseous mixture ionisation to reconstruct the track. Each TS has a large surface area ($r = 8.75$ m) to cover as large a solid angle

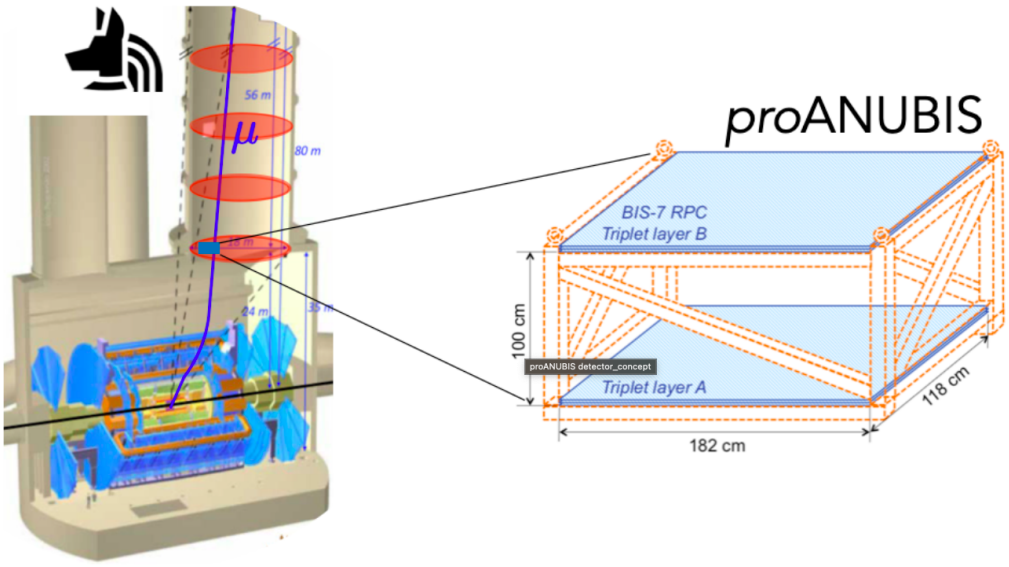


FIG. 4: Schematic diagram of the proposed ANUBIS detector in the ATLAS service shaft with one of the four TSs [9].

as possible. They are both position and time sensitive in order to have efficient track reconstruction with a 0.4 ns time resolution and 0.1 cm spatial resolution. TSs are used in pairs to reconstruct decay vertices happening in the volume between them. First, a signal is measured by a TS after which tracks of LLPs decay products, as well as their decay vertex, are reconstructed. It is then possible to estimate the invisible (because neutral) decaying particle's track, by setting the condition of no hits in the previous TS. As such, decays happening before the first TS are usually not considered in the sensitivity estimate studies due to the absence of a previous detector subsystem in which to check the no-hit condition. This is the Shaft Only (SO) scenario. However, a more optimistic scenario of ANUBIS, called Cavern plus Shaft (C+S) can be considered. Here, ATLAS' MS is taken as an "additional TS", provided that the background sufficiently screened.

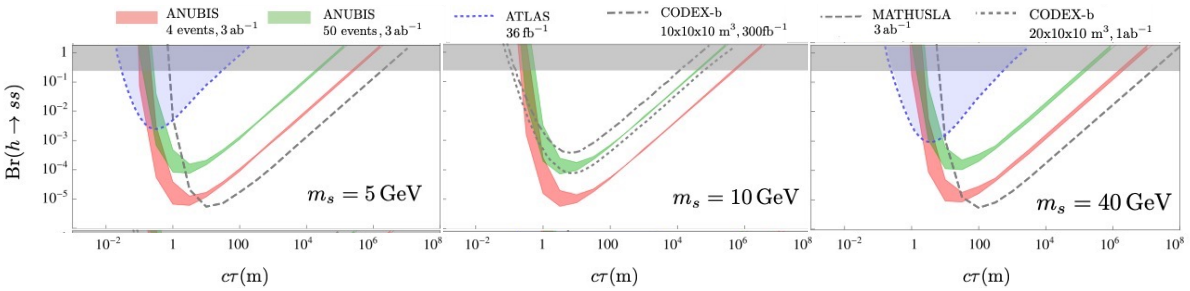


FIG. 5: Sensitivity estimate of ANUBIS in exotic Higgs decay ($h \to ss$) compared to ATLAS, MATHUSLA and CODEX-b[9].

### 2.2.2 Background Estimate

Background in ANUBIS is expected to be very contained. The greatest contribution to the background comes from decays or scatterings of $K_L$ or $n$ inside ANUBIS fiducial volume. However, the probability of them reaching ANUBIS is very low because of the solid angle covered by the detector, which is only a small portion of the total. The already very small amount of background that manages to reach ANUBIS is further reduced by the screening effect of the ATLAS detector. In fact, the calorimeter effectively acts as a "shield" to ANUBIS, promoting strong and hadronic interaction of the particles. The tendency of the calorimeter to promote particles showers can be used as an advantage to exclude or confirm LLP candidates detected by ANUBIS.

## 2.3 Purposes and Perspectives

In Fig. 5, ANUBIS expected sensitivity is shown, compared to ATLAS, MATHUSALA and CODEX-b searches as presented by the ANUBIS proposal paper [9]. These estimates result from simulations of exotic Higgs decay to long lived scalars ($h \to ss$) in two different scenarios: an optimistic one requiring 4 signal events for sensitivity and a conservative one requiring 50. In both cases, the green and red areas are outlined by two curves representing the sensitivity of two setups. The first one employs all four TSs as detection surfaces and requires the no-hits condition to be satisfied at minimum in the first TS, resulting in the active volume corresponding to the shaft's volume (SO). The second one only considers the first TS and employs ATLAS MS to check the absence of previous hits to reconstruct a track. This is the Single Ring (SR) setup which implies taking a section of ATLAS cavern as the active volume while considering the same solid angle subtended by ANUBIS. It can be observed that at low $c\tau$ the second setup performs better. This is because particles with shorter lifetimes will most probably decay in the cavern and are thus only detected if that volume is included in the active region. However, even at longer lifetimes, the curves describing the two setups almost overlap, suggesting that having the

active volume extend so far away from the interaction point is not strictly necessary to achieve high sensitivity.

With this in mind, this investigation will focus on how to maximise ANUBIS sensitivity varying the overall geometry of the detector. In particular I will look at how sensitivity would change as a result of placing the TS over the ceiling in the ATLAS cavern rather than inside the shaft. This will allow to cover a larger solid angle and possibly detect more events. In Fig. 4, it can be seen that in the current proposal ANUBIS only covers a small fraction of the total surface area of the ATLAS cavern. It is trivial to show that, placing the TSs on the ATLAS ceiling would largely increase the total area $A$ of detection while also decreasing the radial distance $R$ from the ATLAS interaction point. Thus, my focus is to assess whether the drastically larger solid angle of the new geometry is enough to improve the sensitivity, even when counteracted by shorter decay lengths with respect to the C+S scenario.

# 3 Methodology

In this study I conducted an investigation on ANUBIS sensitivity and how it varies in different setup scenarios. With this purpose, I created estimates of ANUBIS sensitivity to neutral LLPs coming from exotic higgs decay $h \to ss$ for various geometric setups. The ultimate goal was to assess ANUBIS sensitivity when it consists of a single TS covering ATLAS cavern ceiling and two circular TSs at the PX14 and PX16 shaft's opening, as shown in Fig. 6b, and compare it to the original C+S setup in Fig. 6a.

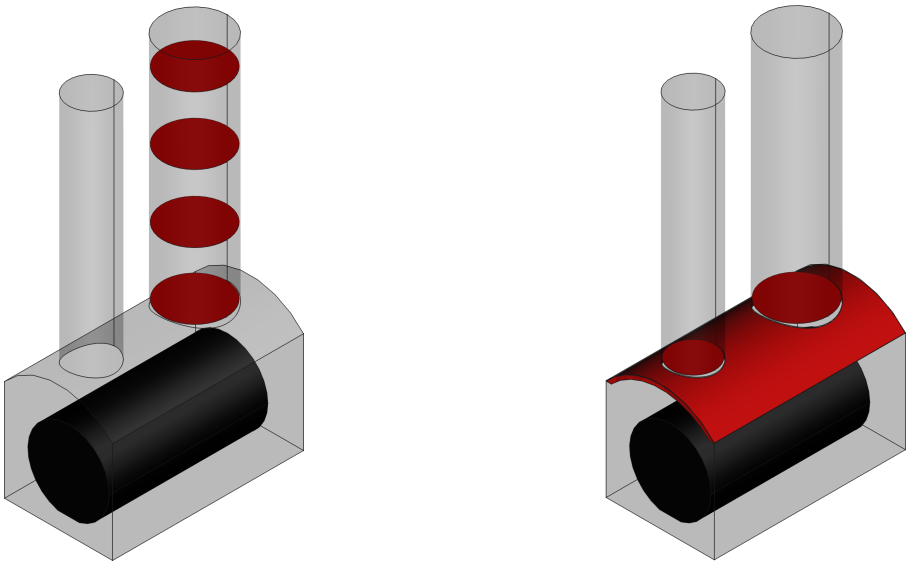

(a) (b)

FIG. 6: Diagram of (a) original ANUBIS C+S setup and (b) proposed alternative geometry with TSs on cavern's ceiling.

## 3.1 Sensitivity Plots

The first step towards creating the sensitivity plots was estimating the number of $h \to ss$ events happening within the active volume assuming BR=1. With this purpose, I employed a set of Les Houches Event (LHE) [18] signal files containing the input Higgs events [19, 20]. These were divided into two datasets, containing Gluon-Gluon fusion and Vector-Boson fusion produced Higgs bosons at $\sqrt{s}$ =13 TeV. The $h \to ss$ decay to neutral LLPs was performed using a Monte Carlo simulation in PYTHIA [21], with chosen LLP masses of 5, 10, 40 and 55 GeV. Requiring the LLP to be produced within the ATLAS volume, it is possible to detect them with ANUBIS via their decay products, provided that any charged daughter can be detected and that the decay happens within the active volume. For each geometrical setup of ANUBIS considered, a cutflow was created for a specific value of the BSM LLP decay length $c\tau$. The first two cuts applied were the angular constraints ($\cos\theta$ and $\phi$), which make sure the LLPs' tracks are actually directed towards ANUBIS. The missing momentum $E_{\mathrm{T}}^{\mathrm{miss}}$ cut was then performed, which was required to be $> 30$ GeV. The next cuts applied were the active volume, which makes sure the decay happened within the signal region, and the no jets condition, as these usually come from hadronisation which constitutes background. Finally 3 independent cuts were executed to obtain the number of charged LLPs, neutral LLPs and no-jets associated neutral LLPs, the latter being the main focus of this work. From such cutflows, the expected number of LLPs detected by ANUBIS $n_{\mathrm{cutflow}}$ can be extrapolated for $\mathrm{BR}(h \to ss) = 1$. Using this, one can trivially obtain the BR corresponding to detection of $n$ events, the number of events required to identify new physics, as $\mathrm{BR}(h \to ss) = n/N_{\mathrm{cutflow}}$. Here $N_{\mathrm{cutflow}}$ is the number of $h \to ss$ events obtained from the cutflow $n_{\mathrm{cutflow}}$ multiplied by the predicted integrated luminosity $L_{\mathrm{int}} = 3\mathrm{ab}^{-1}$ and the relevant Higgs production cross section at $\sqrt{s} = 13$ TeV ($\sigma_{\mathrm{GGF}} = 48.61$ pb and $\sigma_{\mathrm{VBF}} = 3766$ fb [22]), and normalised to the sum of all of the events weights. In this investigation two scenarios were considered in which $n$ is 4 (optimistic scenario) and 50 (conservative scenario). The motivation for the first of these arises from the wish to compare the estimates to the MATHUSLA and CODEX-b ones which used the same $n$, and is only relevant if background levels are particularly low. The 50 events scenario is instead taken from the ATLAS MS search [23], assuming the same level of background.

Repeating this procedure for a range of LLPs' decay lengths $c\tau$ up to $10^8$ m, sensitivity estimates can be created plotting the resulting $\mathrm{BR}(h \to ss)$ as a function of $c\tau$. These were produced for various different geometries and, in most cases, compared to the original C+S scenario in Fig. 6a.

## 3.2 Geometry Optimisation

To study ANUBIS sensitivity I first reproduced the already existing plots for the two original scenarios SO and C+S for LLP masses of 5, 10 and 40 GeV. Then, I started altering the setup and extrapolated the number of detected events for each one to analyse the corresponding changes in sensitivity. In particular I initially looked at the SR scenario. The question on ATLAS radius was then raised, motivated by the fact that we are now considering the MS as an additional tracking device. The size of the active volume, and thus the sensitivity, would in fact drastically depend on the choice of the ATLAS radius considered, which is why I conducted a brief investigation on the how changing it would affect the BR curves. The radii considered were the endcap radius, $R_{\text{ATLAS}} = 12.5$ m, the barrel radius, $R_{\text{ATLAS}} = 10$ m and the vertexing efficiency boundary radius, $R_{\text{ATLAS}} = 7$ m [24]. Ultimately, I chose the better performing one for my studies, i.e. $R_{\text{ATLAS}} = 7$ m. The following step was the implementation of the script which I used, with variations, for all the geometric setups considered . In particular, I modified the active volume cut in the original script [1] to check which particle tracks intercepted the relevant TS and then return the resulting number of valid events. With this new code I was able to obtain sensitivity plots for a various range of geometric setup starting by considering a square TS with side $l = 17$ m at the centre of the cavern (Fig. 7a). The trajectories of the particles were modeled as straight lines passing through the origin and a point on the surface of a sphere, centred at the ATLAS IP. Thus, all tracks are described by two coordinates: the angle $\theta$ to the beam axis z (from which the pseudorapiditiy $\eta$ is obtained) and the angle $\phi$ in the $x - y$ plane ($x$ being parallel to the shaft). Of these tracks, only those that intersect the square TS at an height of $x = 24$ m right above the IP were selected as ANUBIS events, from which the sensitivity estimate was obtained as detailed above. In an attempt to gain an understanding of the sensitivity of the proposed final setup in Fig. 6b I increased the surface area of ANUBIS, setting it to be a rectangular TS the size of the ceiling (i.e. $53 \times 28.7$ m$^2$) at an height of $x = 20$ m (Fig. 7b) and created the relevant sensitivity plot. I then investigated the geometry shown in Fig. 7c, which was implemented by requiring intersection of the tracks with a section of a cylinder with radius equal to the cavern curvature radius $r$ =20 m. I then applied the cuts shown in Fig. 7d to this geometry, corresponding to where the openings of the PX14 and PX16 shafts are. The final step in the study was adding two TS at the bottom of the two shafts, which were modeled as two circles with $r_{\text{PX14}} = 8.75$ m and $r_{\text{PX16}} = 6.05$ m, at a height of $x = 24$ m. This corresponds to the diagram in Fig. 6b. The resulting sensitivity estimate was compared to the original C+S scenario.

[1] The original scripts were provided by Dr. Jonathan Burr.

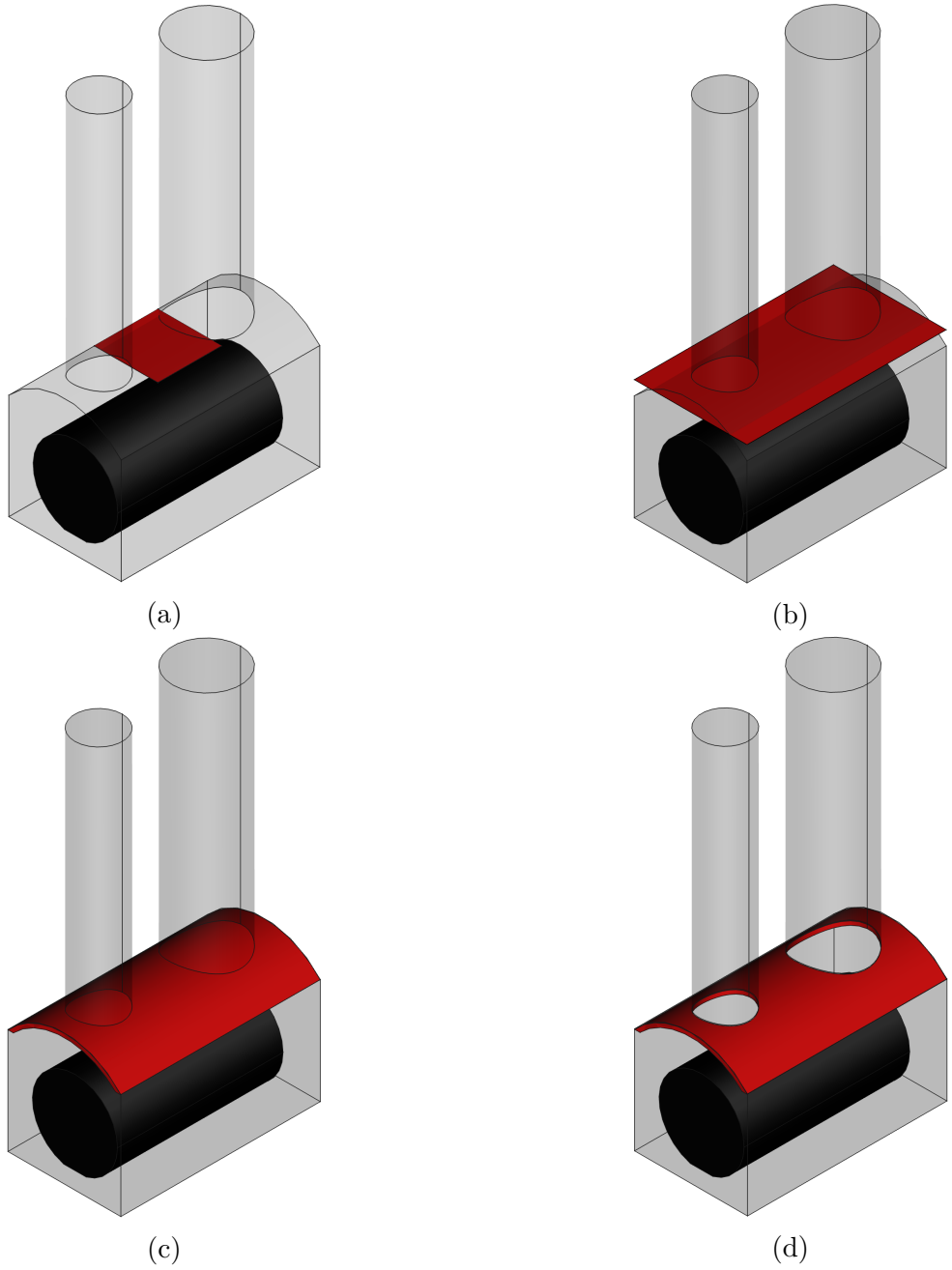

FIG. 7: Diagram of ANUBIS as (a) a square TS with side $l = 17$ m at the centre of the cavern (b) a plane TS the size of ATLAS' cavern, (c) a curved TS corresponding to the cavern's ceiling and (d) a curved TS corresponding to the cavern's ceiling with cuts for the PX14 and PX16 shafts.

# 4 Results and Discussion

Here I discuss all the results of the investigation. In section 4.1 I reproduce the original setup sensitivity estimates for $m_{\text{LLP}} = 10$ GeV with slight modifications to the ATLAS radius considered. In section 4.2 I present the sensitivity plots I produced for the various geometric setups considered throughout the investigation process for LLP mass of 10 GeV. In section 4.3 I display the sensitivity estimates for the final geometry with the whole ceiling as tracking surface for all masses considered: 5, 10, 40 and 55 GeV. In App. A I also show the breakdown of sensitivity estimates for the GGF and VBF produced Higgs for the 10 GeV LLP. It is relevant to mention that an error analysis was conducted when creating the sensitivity estimates, considering the statistical uncertainty in event generation and the experimental error on the Higgs production cross sections [22]. The results these produced were however very small and not visible in the plots, which is why they are not included in this report.

## 4.1 Original Setup

As detailed in section 3.1, the first step in the investigation was creating cutflows at various decay lengths and reproducing the already existing sensitivity plots. Figure 8 displays one of such cutflow, created for an LLP of $m = 10$ GeV and $c\tau = 10$ m for the original C+S geometric setup. From the last cut, I extracted the number of events corresponding to neutral LLPs that are not associated to a jet.

In Fig. 9 I reproduced, as a check, the sensitivity plot of the original setup, showing ANUBIS sensitivity estimates for $m_{\text{LLP}} = 10$ GeV. The same plots for LLP masses of 5 and 40 GeV are shown in App. B. Specifically, the top curve represents the sensitivity of the SO scenario, which increases up to the bottom curve when considering ATLAS cavern as active volume in the C+S scenario. As expected, we observe an overall higher sensitivity as a consequence of the increase in active volume. In particular, ANUBIS gets significantly more sensitive to particles with lower $c\tau$, since regions closer to the IP, where their decay happens, are being considered.

In Fig. 10, the SR scenario already displayed in Fig. 5 was reproduced and compared to the C+S. Here we see consistency between the existing (Fig. 5) and new results with the two plots agreeing to a peak in sensitivity of $\text{BR}(h \to ss)_{n=50} \approx 1.5 \times 10^{-4}$ and $\text{BR}(h \to ss)_{n=4} \approx 10^{-5}$ at $c\tau = 3$ m. When compared to the C+S scenario we can see agreement between the two curves at low $c\tau$. This was expected since up until the first TS ($\approx 20$ m from the IP) the same active volume is considered. However, C+S is naturally more sensitivity to larger $c\tau$ as it extends further away from the IP.

As mentioned above, extending the active volume up until ATLAS detector drastically

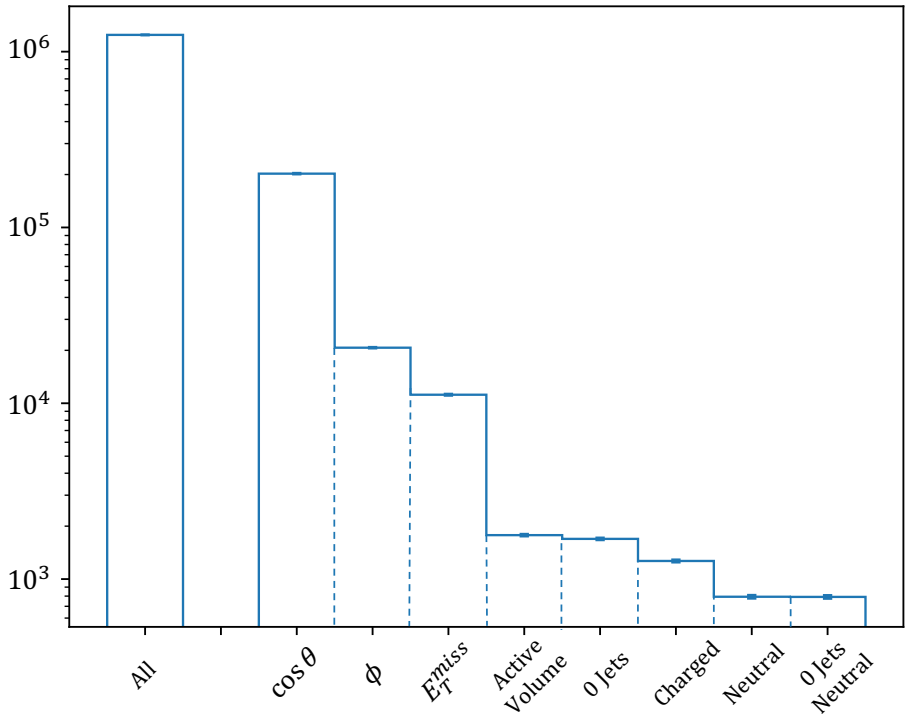


FIG. 8: Cutflow at $c\tau = 10$ m for an LLP of $m = 10$ GeV with $E_{\mathrm{T}}^{\mathrm{miss}} > 30$ GeV for C+S setup.

affects the sensitivity estimate, which will be highly dependent on the choice of its radius. Thus, Fig. 11 displays the C+S sensitivity when considering variations in the radius of ATLAS. As expected, when decreasing the radius from $R_{\mathrm{ATLAS}} = 12.5$ m to $R_{\mathrm{ATLAS}} = 7$ m, it is possible to observe an increase in sensitivity of about 1/4 of a order of magnitude at the sensitivity peak. This is trivially explained by that fact that decreasing ATLAS radius will increase the active volume, thus allowing more events to be detected by ANUBIS. Considering this, henceforth, all results presented assume an ATLAS radius of $R_{\mathrm{ATLAS}} = 7$ m, thus displaying the most optimistic of scenarios.

## 4.2 Intermediate Geometries

Throughout this work, various intermediate geometries were investigated leading up to the final setup which I present in this section. Fig. 12 shows the sensitivity estimate obtained for a single square TS placed at the centre of the ATLAS cavern, as shown in Fig. 7a, and compares it to the C+S scenario. As in the SR case, we find agreement with expectations, where the C+S performs better at large lifetimes, due to the presence of TS further away from the IP. On the other hand, at low $c\tau$ the two plots are consistent, as they both include the cavern as active volume.

Fig. 13 shows the sensitivity estimate for a rectangular TS ($53 \times 28.7$ m$^2$) covering the entire cavern ceiling, placed midway through the curved section of the ceiling, as shown

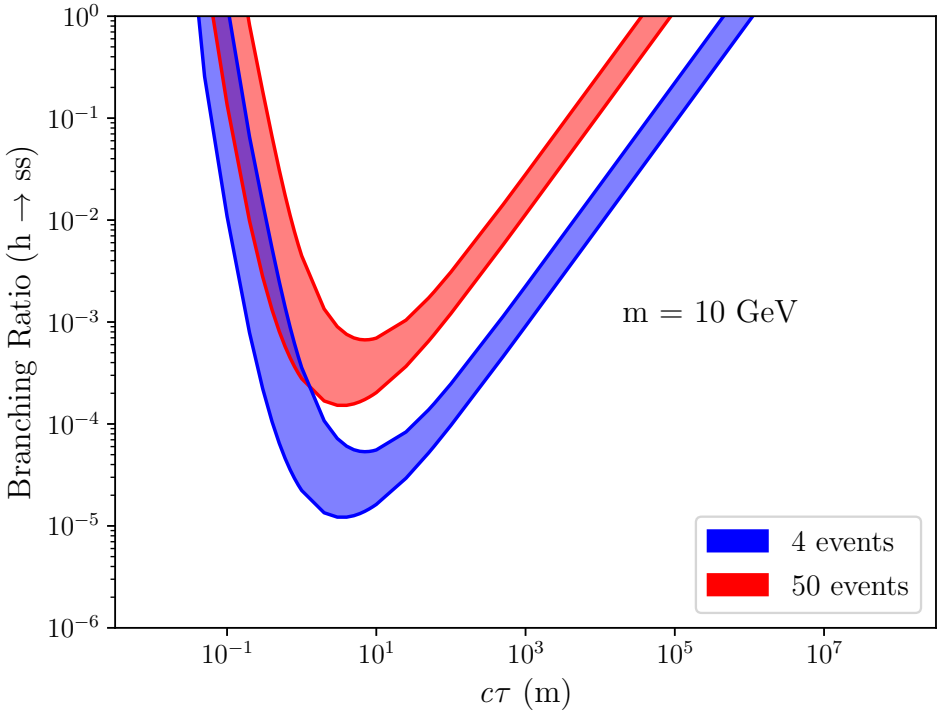


FIG. 9: Sensitivity of the two original setups SO (top curve) and C+S (bottom curve) for LLP mass of 10 GeV.

in Fig. 7b. The curve was compared to the square TS sensitivity shown above, to check the relation between surface area and sensitivity. Table 1 reports the values of the surface area, along with the corresponding sensitivity peak, for the two setups. It can be observed

| | Ceiling TS | Square TS | Ratio |
|---|---|---|---|
| Area ($m^2$) | 1473.4 | 289 | 5.1 |
| BR($h \to ss)_{50}$ | $2.8 \times 10^{-5}$ | $1.2 \times 10{-}4$ | 4.3 |

TABLE 1: Surface areas of Ceiling TS and Square TS with their ratio, along with corresponding peaks in sensitivity and their ratio.

that an increase in surface area is affecting almost linearly the corresponding sensitivity, with the areas and sensitivities ratios being very close in value. The variation in the ratio can be easily explained by the fact that the rectangular TS, in addition to being bigger, also extends further away from the detector, meaning that there would be an improved sensitivity at large $c\tau$ when compared to the $17 \times 17$ $m^2$ TS.

In Fig. 14 I modified the ceiling TS shown above to follow the curvature of the cavern ceiling, taking into account the displacement of 1.7 m of the ATLAS IP with respect to the centre of the cavern. The geometric set up is shown in Fig. 7c. The curve is, as expected, very close to the case presented in Fig. 13, with negligible variations due to the slight change in distance from the IP due to the curvature. When compared to the C+S

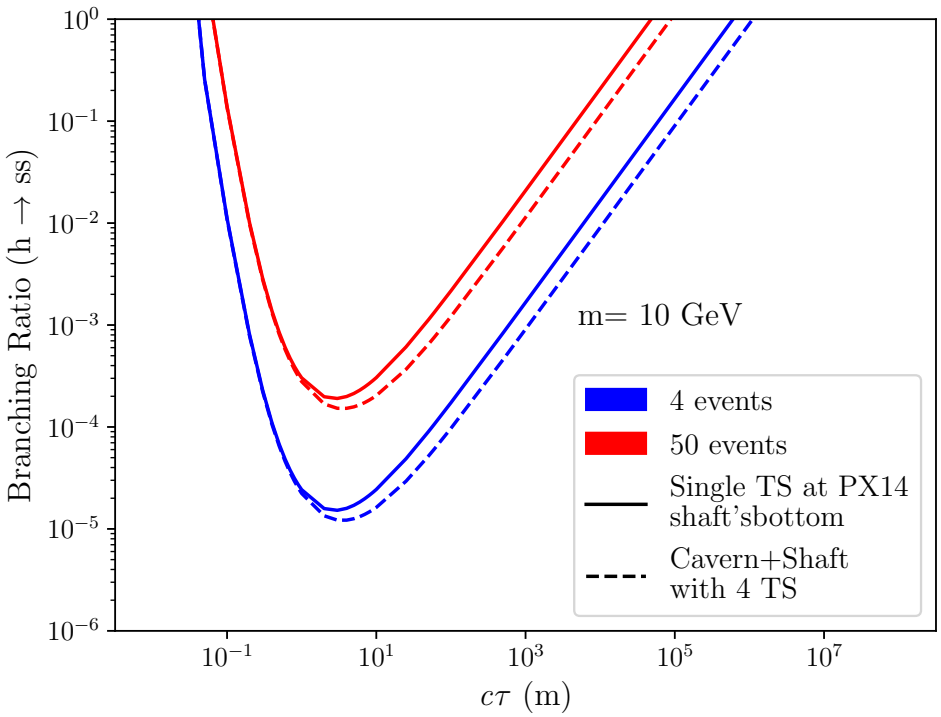


FIG. 10: Sensitivity estimate for SR scenario compared to C+S

scenario, we can see that the ceiling TS performs significantly better, suggesting that the sensitivity is more affected by the size of the solid angle, rather than the distance at which the TS is placed. In particular, it is very interesting and relevant to notice that, even though the C+S setup includes a TS $\approx 80$ m away from the IP, while the ceiling one only extends up until 24 m, a greater sensitivity is achieved by the latter even at large $c\tau$.

The last plot obtained before the final geometric setup is shown in Fig. 15, where I included the cutouts for the 2 access shafts of ATLAS cavern, PX14 and PX16. As expected, we see a decrease in sensitivity with respect to the case shown above due to the smaller surface area, while still observing improved sensitivity with respect to C+S. In Tab. 2 I reported the ratio of areas and sensitivities to check the proportionality between Curved Ceiling with and without cuts. The results are consistent with expectations.

| | Curved Ceiling | Curved Ceiling with Shafts' cutouts | Ratio |
|---|---|---|---|
| Area ($m^2$) | 1696.4 | 1305.6 | 1.3 |
| BR($h \to ss$) | $2.8 \times 10^{-5}$ | $4.5 \times 10^{-5}$ | 1.6 |

TABLE 2: Surface areas of Curved ceiling TS with and without shafts cuts with their ratio, along with corresponding peaks in sensitivity and their ratio.

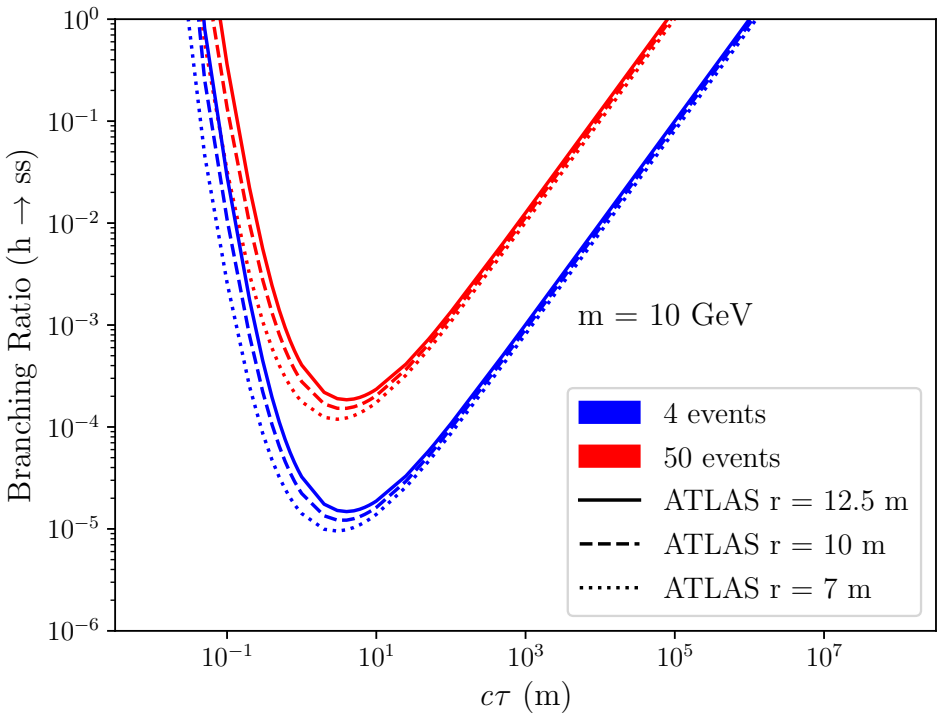


FIG. 11: Effect of changing ATLAS radius on sensitivity estimate of the C+S setup.

### 4.3 Final Geometry

In this section I present the sensitivity estimates of the final geometry considered, involving a large TS covering the cavern ceiling with two circular TS at the openings of the PX14 and PX16 shafts (Fig. 6b). I compare these to the original C+S scenario estimate for masses of 5, 10, 40 and 55 GeV (Fig. 16).

As expected from the intermediate steps shown in Sec. 4.2, for all masses considered we see that, somewhat counter-intuitively, this geometric setup, while not extending particularly away from the IP, performs significantly better than the C+S one for all $c\tau$. This is particularly relevant, not only within the theory, but also on logistic experimental grounds. In fact, in the original ANUBIS proposal, one of the greatest engineering challenges lies in having four TS within the shaft which would need to be removed, and safely stored, in between runs of the LHC to allow for access to the cavern. This would clearly result in a considerable amount of hard work. The new suggested scenario, involving a fixed detector (the ceiling) and only one TS at the bottom of each shaft, significantly reduces the complexities described above. Thus, it is clearly great news that the latter of the two setups performs better.

In addition, comparing the sensitivity estimates to LLPs of different masses, it is possible to observe a shift of the BR curve towards higher $c\tau$ as the mass increases. This has to do with the fact that massive LLPs are significantly less boosted, meaning they will decay sooner (due to less time dilation). This naturally leads to a higher probability

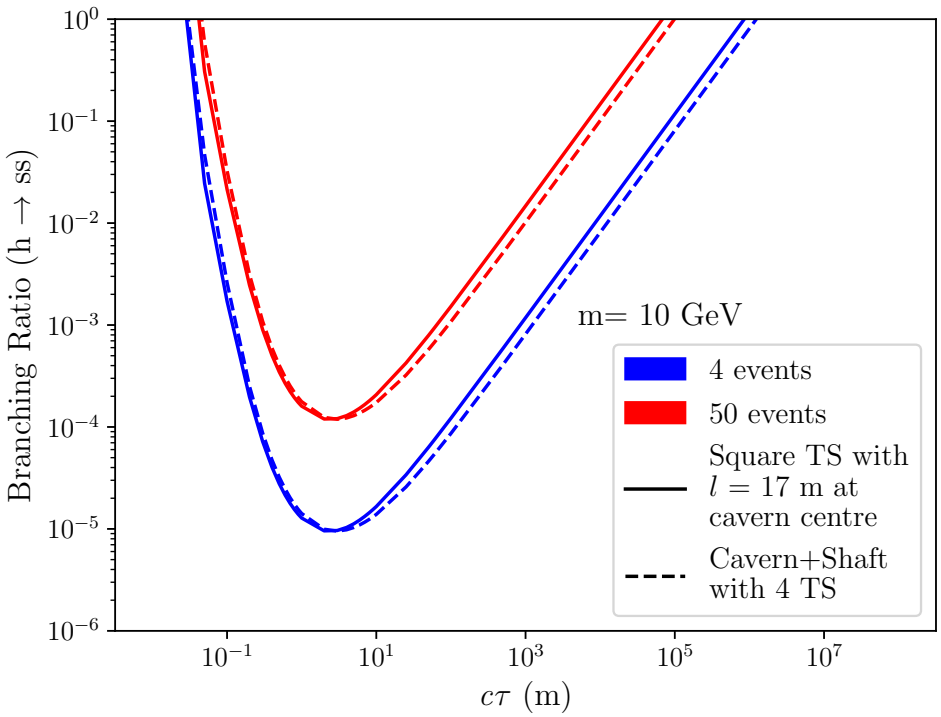


FIG. 12: Sensitivity estimate for square TS of side $l = 17$ m placed at the centre of ATLAS cavern.

of decays happening inside ANUBIS' active volume, thus increasing the sensitivity to longer lifetimes. At the same time, being slower, massive particles with short $c\tau$ will decay closer to the IP, making it more difficult for them to be identified as LLPs via the typical displaced vertex signature. As a consequence, ANUBIS will be less sensitive to low $c\tau$ for massive LLPs, resulting in the observed trend in Fig. 16.

# 5 Conclusions

In this study, I conducted an investigation on the sensitivity of ANUBIS, a new detector that aims to search for LLPs produced in Higgs decays at ATLAS. The experiment plans to instrument ATLAS service shaft with four TS used to identify neutral LLPs via reconstruction of their decay DV.

ANUBIS sensitivity estimates predict it to successfully constrain BRs up to three order of magnitudes lower than ATLAS, even when only one TS is considered. Thus, here I investigated the sensitivity of an alternative geometric setup to the original one involving TSs placed over ATLAS ceiling surface, so as to cover a significantly larger solid angle. To achieve our purpose, a range of intermediate geometries were considered, gradually leading up to the final set up, which involves a large fixed TS covering the ATLAS ceiling and two circular ones at the openings of the PX14 and PX16 shafts. The sensitivity

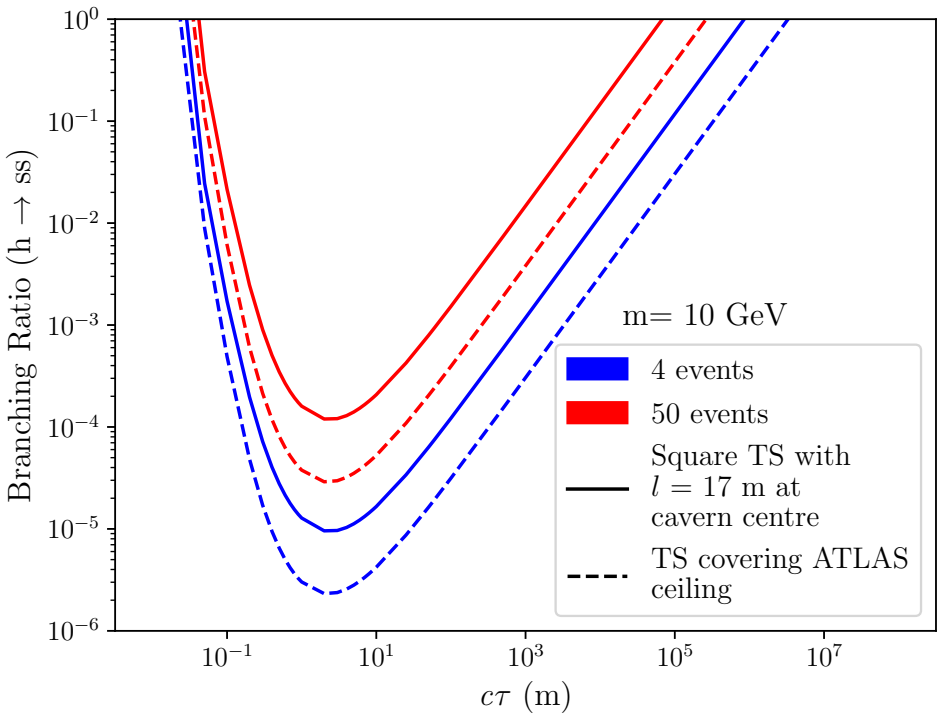


FIG. 13: Sensitivity estimate for plane TS the size of ATLAS cavern ceiling compared to square TS.

estimate for this geometry was shown to perform significantly better than the most optimistic of original ones, improving the constraints by up to an order of magnitude. This is suggestive of the fact that the wider solid angle has a larger impact on the sensitivity than the radial distance, highlighting the fact that high sensitivities can be achieved even without placing tracking sheets very far away from the interaction point. Furthermore, the curves were found to be consistent with expectations in that sensitivity to heavier, and thus slower, LLPs was seen to shift towards higher $c\tau$.

Surely, the proposed alternative geometry for ANUBIS involving the ceiling as additional TS can appear ambitious, also considering the necessary condition of a low background. In particular, it is important to note that in this investigation the number of events required for sensitivity (4 and 50) did not change as a consequence of the increase in solid angle. This is of course not realistic, as a wider solid angle will mean, in addition to more interesting events, more background. Thus, it would be relevant to conduct a further investigation on this geometric set up focusing specifically on the background estimates. Even so, the presented results encourage reflection about the potential of this new setup and its possible employment in future collider experiments (i.e. let's use our ceilings!). Future developments of this investigation could look at sensitivity estimates of a setup with TS placed directly on ATLAS surface, which would drastically reduce the active volume but further increase the solid angle.

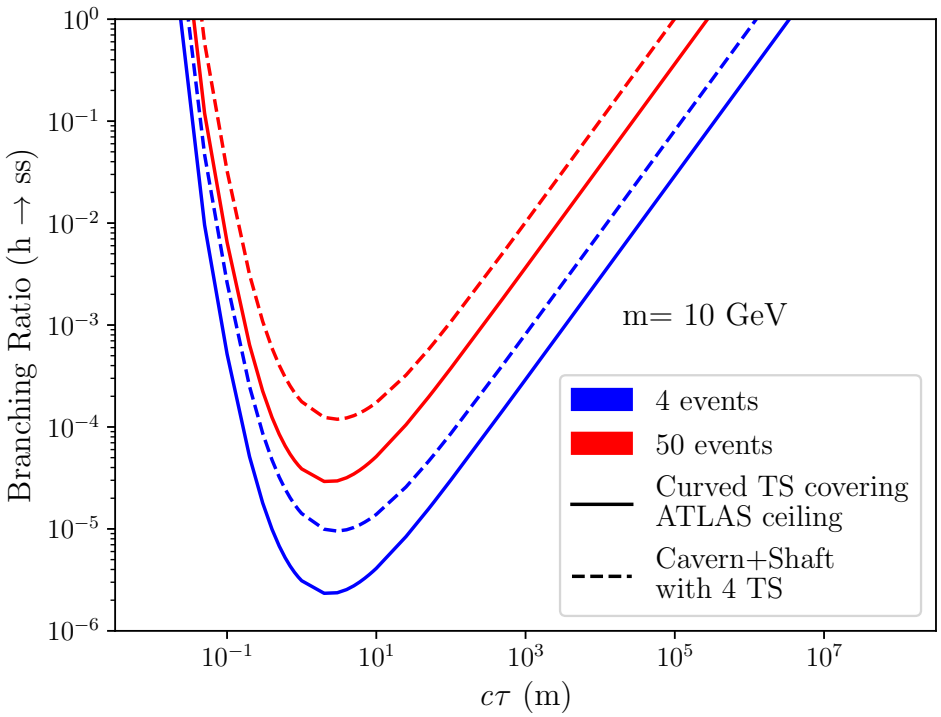


FIG. 14: Sensitivity estimate for curved plane TS the size of ATLAS cavern ceiling compared to C+S.

## Acknowledgements

I would like to thank my supervisor Dr. Oleg Brandt for the invaluable and constant guidance throughout the year. I would also like to thank Dr. Jonathan Burr for the continuous help and advice during the project and for answering my many questions.

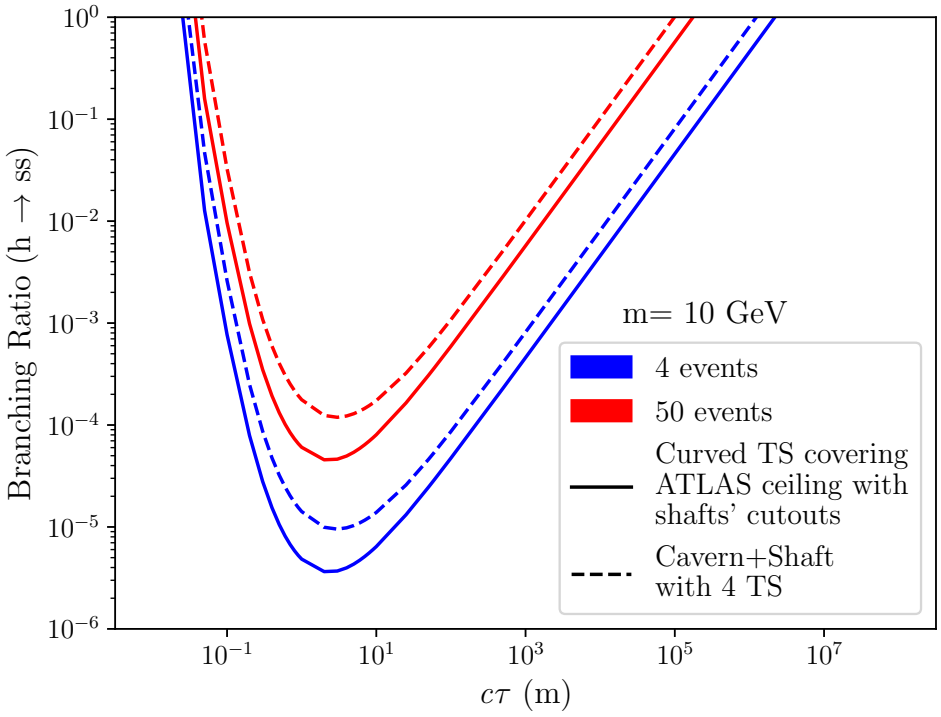


FIG. 15: Sensitivity estimate for curved plane TS on ATLAS ceiling with cuts for shafts compared to C+S.

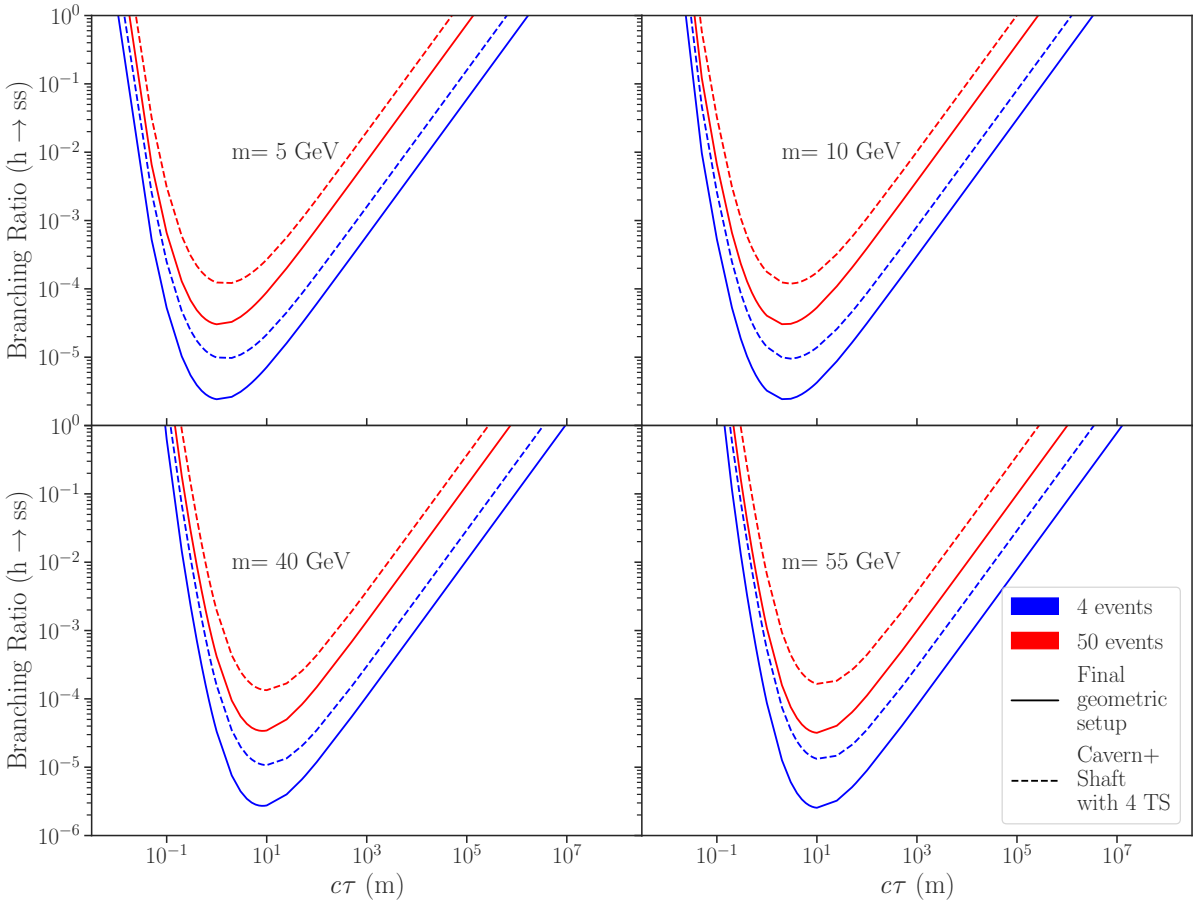


FIG. 16: Sensitivity estimate for final ANUBIS setup for masses of 5, 10, 40 and 55 GeV.

# References


[1] J. Beacham, C. Burrage, *et al.*, "Physics beyond colliders at CERN: beyond the standard model working group report," Journal of Physics G: Nuclear and Particle Physics **47**, 010501 (2019).

[2] S. Argyropoulos, O. Brandt, and U. Haisch, "Collider Searches for Dark Matter through the Higgs Lens," arXiv preprint arXiv:2109.13597 (2021).

[3] G. Aad, , *et al.* (ATLAS Collaboration), "The ATLAS experiment at the CERN large hadron collider," (2008).

[4] S. Chatrchyan *et al.* (CMS Collaboration), "The CMS experiment at the CERN LHC," (2008).

[5] A. A. Alves Jr *et al.*, "The LHCb detector at the LHC," Journal of instrumentation **3**, S08005 (2008).

[6] J. P. Chou, D. Curtin, and H. Lubatti, "New detectors to explore the lifetime frontier," Physics Letters B **767**, 29 (2017).

[7] V. V. Gligorov, S. Knapen, M. Papucci, and D. J. Robinson, "Searching for long-lived particles: a compact detector for exotics at LHCb," Physical Review D **97**, 015023 (2018).

[8] A. Ariga, T. Ariga, *et al.*, "FASER: forward search experiment at the LHC," arXiv preprint arXiv:1901.04468 (2019).

[9] M. Bauer, O. Brandt, L. Lee, and C. Ohm, "ANUBIS: Proposal to search for long-lived neutral particles in CERN service shafts," arXiv preprint arXiv:1909.13022 (2019).

[10] D. Curtin, M. Drewes, M. McCullough, *et al.*, "Long-lived particles at the energy frontier: the MATHUSLA physics case," Reports on progress in physics **82**, 116201 (2019).

[11] D. Curtin, R. Essig, S. Gori, *et al.*, "Exotic decays of the 125 GeV Higgs boson," Physical Review D **90**, 075004 (2014).

[12] G. Aad *et al.* (ATLAS Collaboration), "Observation of a new particle in the search for the Standard Model Higgs boson with the ATLAS detector at the LHC," Physics Letters B **716**, 1 (2012).

[13] S. Chatrchyan *et al.* (CMS Collaboration), "Observation of a new boson at a mass of 125 GeV with the CMS experiment at the LHC," Physics Letters B **716**, 30 (2012).

[14] Z. Chacko, H.-S. Goh, and R. Harnik, "Natural Electroweak Breaking from a Mirror Symmetry," Physical Review Letters **96** (2006), 10.1103/physrevlett.96.231802.

[15] G. Burdman, Z. Chacko, H.-S. Goh, and R. Harnik, "Folded supersymmetry and the LEP paradox," Journal of High Energy Physics **2007**, 009 (2007).

[16] H. Cai, H.-C. Cheng, and J. Terning, "A quirky little Higgs model," Journal of High Energy Physics **2009**, 045 (2009).

[17] L. Lee, C. Ohm, A. Soffer, and T.-T. Yu, "Collider searches for long-lived particles beyond the Standard Model," Progress in Particle and Nuclear Physics **106**, 210 (2019).

[18] J. Alwall, A. Ballestrero, *et al.*, "A standard format for Les Houches event files," Computer Physics Communications **176**, 300 (2007).

[19] P. Nason and C. Oleari, "NLO Higgs boson production via vector-boson fusion matched with shower in POWHEG," JHEP **02**, 037 (2010).

[20] P. Nason, "A new method for combining NLO QCD with shower Monte Carlo algorithms," JHEP **11**, 040 (2004), arXiv:hep-ph/0409146 .

[21] T. Sjöstrand, S. Ask, J. R. Christiansen, R. Corke, N. Desai, P. Ilten, S. Mrenna, S. Prestel, C. O. Rasmussen, and P. Z. Skands, "An introduction to PYTHIA 8.2," Comput. Phys. Commun. **191**, 159 (2015), arXiv:1410.3012 [hep-ph] .

[22] M. Cepeda, S. Gori, *et al.*, "Higgs physics at the HL-LHC and HE-LHC," arXiv preprint arXiv:1902.00134 (2019).

[23] M. Aaboud, G. Aad, *et al.*, "Search for long-lived particles produced in p p collisions at $\sqrt{s} = 13$ TeV that decay into displaced hadronic jets in the ATLAS muon spectrometer," Physical Review D **99**, 052005 (2019).

[24] G. Aad *et al.* (ATLAS Collaboration), "Search for events with a pair of displaced vertices from long-lived neutral particles decaying into hadronic jets in the ATLAS muon spectrometer in pp collisions at $\sqrt{s}$ =13 TeV," arXiv preprint arXiv:2203.00587 (2022).

# A GGF vs VBF

Fig. 17 shows the breakdown of the final setup's sensitivity to GGF and VBF produced Higgs decaying to a 10 GeV LLP. Looking at Fig. 17 and Tab. 3, which displays the BR of

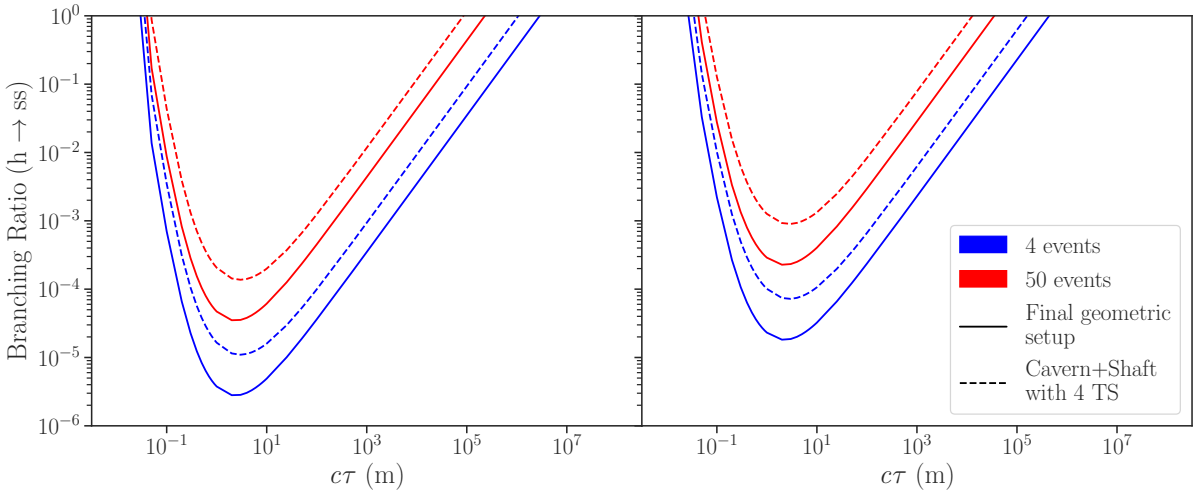


FIG. 17: Breakdown of sensitivity Estimate of final geometry for GGF left and VBF right produced Higgs.

the peaks, it can be noted that the GGF contribution is significantly more relevant. This

| | C+S 4 events | C+S 50 events | Final 4 events | Final 50 events |
|---|---|---|---|---|
| GGF | $1.1 \times 10^{-5}$ | 0.000137 | $2.8 \times 10^{-6}$ | $3.5 \times 10^{-5}$ |
| VBF | $7.2 \times 10^{-5}$ | 0.00090 | $1.8 \times 10^{-5}$ | 0.00022 |

TABLE 3: Breakdown of limits peak on Branching Ratio for GGF and VBF for C+S and Final geometric setups.

is easily explained by the fact that the Higgs production cross section at $\sqrt{s} = 13$ TeV for VBF is $\sigma_{VBF} = 3766$ fb, an order of magnitude smaller than the GGF one $\sigma_{GGF} = 48.61$ pb [22], which well agrees with the trend shown in the plot and table.

# B Remaining Sensitivity Results

Here I present the sensitivity estimates for the two original setups (SO and C+S) for the 5 and 40 GeV LLPs (Fig. 18). The plots are consistent with the result shown previously, showing an increase in sensitivity when including the ATLAS cavern in the active region, especially at low $c\tau$ . Also, as presented in Fig. 16, we observed a shift towards higher $c\tau$

as the mass of the LLP increases, which is explained by the same reasonings presented in Sec. 4.3.

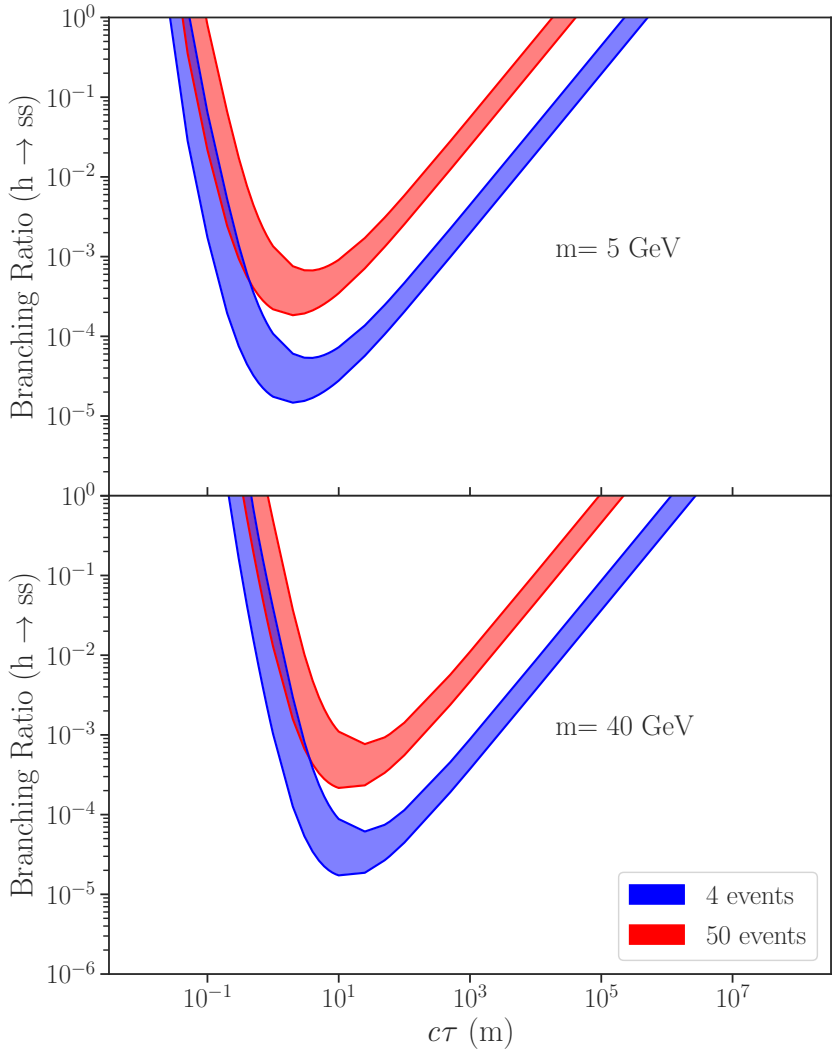


FIG. 18: Sensitivity of the two original setups SO (top curve) and C+S (bottom curve) for LLP masses of 5 and 40 GeV.